Analysis and Tuning of a Flyweight-Actuated Continuously Variable Transmission

Brendon Anderson*

4 February 2017

Abstract

In this report, the mechanics of a flyweight-actuated continuously variable transmission are examined using quasi-static analysis. After mathematically modeling the belt kinematics, as well as the primary and secondary clutch mechanisms, the input and output states of the transmission are coupled to produce a single equilibrium equation. Finally, a MATLAB implementation of the equilibrium equation is presented as a means to tune the CVT to operate at the desired engine speed.

1 Introduction

1.1 Motivation

The transmission of power from the output of an automotive engine to the input of the wheels is a topic of great concern to all kinds of drivers. Whether the vehicle is used to commute to work or race for thrills, any method by which the efficiency of its drivetrain can be increased is worthy of pursuit. Continuously variable transmissions (CVTs) are v-belt systems which utilize adjustable pulleys that allow for the smooth and continual change in transmission ratio. This feature permits the engine to rotate at a constant speed while the vehicle accelerates by gradually shifting ratios, rather than sequencing through a series of discrete gear ratios, as in the ubiquitous automatic and manual transmissions of the previous century. By tuning the CVT to operate at an engine speed that yields either optimal fuel efficiency or peak power, various sorts of drivers can find a direct benefit in the use of continuously variable transmissions.

Though their low cost and high reliability are desirable, mechanically actuated CVTs can provide troubles when a technician is faced with tuning them. Trial-and-error adjustment of their configurations is undoubtedly a cumbersome process. This report aims to mathematically model the mechanisms found in the most common form of mechanically actuated CVTs in order to develop a more systematic approach to achieving the desired tuning configuration, specifically in the form of a simple MATLAB program.

1.2 System Description

The system to be analyzed is a mechanically actuated v-belt CVT. Each of the two pulleys are composed of one moveable and one axially fixed conical sheave, also known as a half-pulley. The pulley attached to the output shaft of the engine is termed the primary clutch, and houses the

*Bruin Racing | Baja SAE at University of California, Los Angeles

mechanism used to activate transmission ratio changes. The actuation takes effect through the clever placement of ramps within the primary clutch cage. Inside the primary clutch cage resides a number or radially spaced lever arms with masses at their ends. These flyweights, when subjected to an increase in engine speed, ride along the primary ramps due to centripetal effects which in turn causes the moveable sheave to increase the radius at which the belt rides on the primary pulley. Due to the finite length of the v-belt, the belt radius at the secondary pulley, or output clutch, must decrease. The shift in gear ratio causes the engine speed to decrease to the rate at which it was at prior to the shift. This feedback phenomena is what allows for the CVT to operate at a constant engine speed within its range of transmission ratios.

The specific CVT model used in this report is the Gaged GX9. The GX9 is intended for use in small vehicles, and is a popular choice by Baja SAE race teams around the world.

2 Analytical Development

2.1 V-Belt Kinematics

2.1.1 Belt Length

The current model will be developed under the assumption of an inextensible belt. While shifting, any change in belt radius at the primary clutch must be counteracted by an opposing change in belt radius at the secondary clutch in order to maintain a constant overall belt length. Therefore, after the belt has been engaged by the primary pulley, the radii at the two clutches can be directly related through the geometry shown in Figure 1.

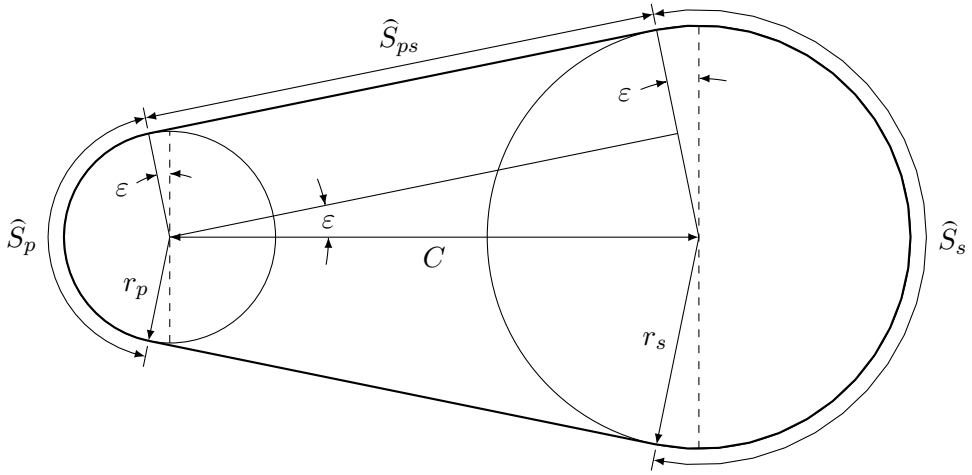

Figure 1: Geometric relation between belt length and pulley radii.

The length of the belt can be expressed as

$$L_b = \widehat{S}_p + \widehat{S}_s + 2\widehat{S}_{ps},$$

where the arc lengths of interest are

$$\begin{aligned}
\widehat{S}_p &= (\pi - 2\varepsilon) r_p, \\
\widehat{S}_s &= (\pi + 2\varepsilon) r_s, \\
\widehat{S}_{ps} &= \left(C^2 - (r_s - r_p)^2\right)^{1/2}.
\end{aligned}$$

Thus,

$$L_b = (\pi - 2\varepsilon)r_p + (\pi + 2\varepsilon)r_s + 2\Big(C^2 - (r_s - r_p)^2\Big)^{1/2},$$

where

$$\varepsilon = \arcsin\left(\frac{r_s - r_p}{C}\right). \tag{1}$$

Therefore, for a known belt length and center-to-center distance between clutches, an implicit relationship between r_p and r_s can be written as

$$L_b = \pi(r_p + r_s) + 2(r_s - r_p)\arcsin\left(\frac{r_s - r_p}{C}\right) + 2\Big(C^2 - (r_s - r_p)^2\Big)^{1/2}. \tag{2}$$

2.1.2 Sheave Displacement

Figure 2 shows the geometric relation between an incompressible v-belt of width w_b and the adjustable primary-side pulley on which it rides. Note that one sheave is fixed axially.

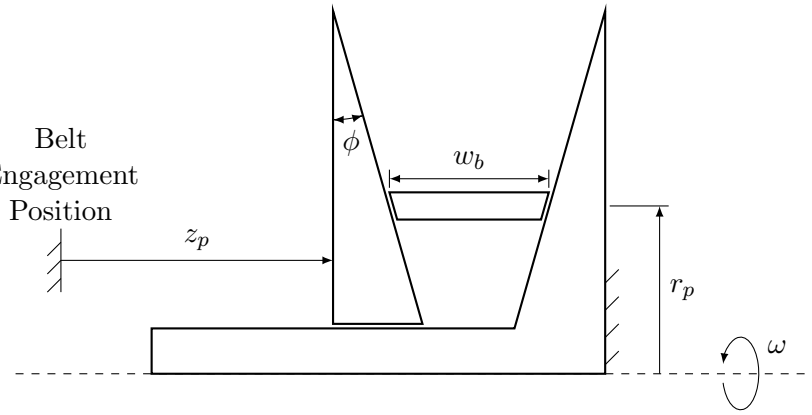

Figure 2: V-belt geometry after belt engagement.

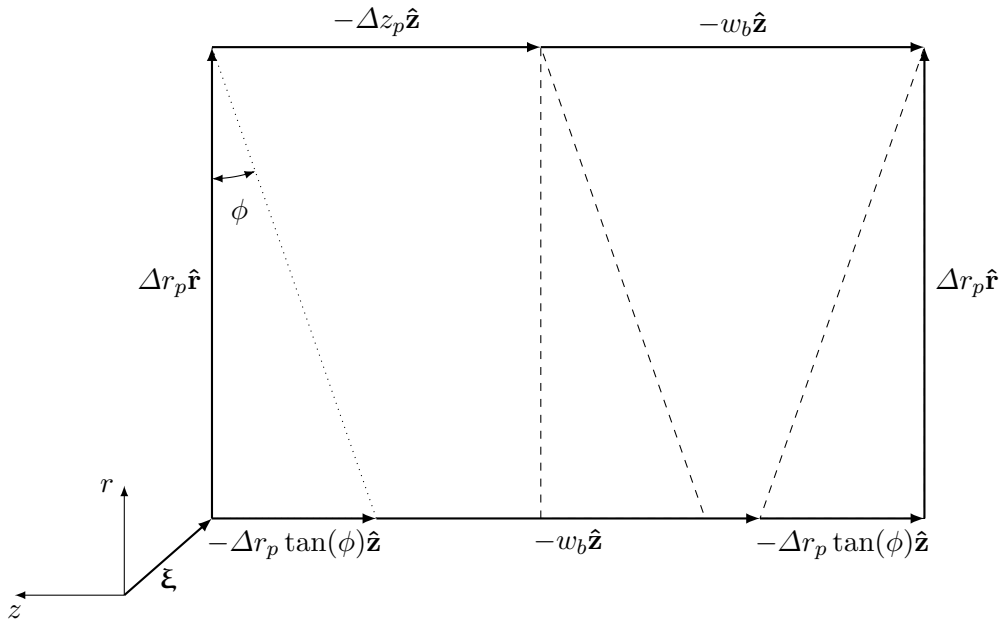

Figure 3: Vector analysis of v-belt shifting.

As shown in Figure 3, the belt must ride to a larger radius as the gap between the sheaves decreases. Simple vector analysis gives

$$\boldsymbol{\xi} + \Delta r_p\hat{\mathbf{r}} - \Delta z_p\hat{\mathbf{z}} - w_b\hat{\mathbf{z}} = \boldsymbol{\xi} - \Delta r_p\tan(\phi)\hat{\mathbf{z}} - w_b\hat{\mathbf{z}} - \Delta r_p\tan(\phi)\hat{\mathbf{z}} + \Delta r_p\hat{\mathbf{r}}.$$

Thus, the change in axial position of the moveable sheave in terms of change in belt radius is

$$\Delta z_p = 2\Delta r_p\tan(\phi).$$

By taking $z_p = 0$ at the position of belt engagement, and denoting the belt radius at that instant by $r_{p,eng}$, this result becomes

$$z_p = 2(r_p - r_{p,eng})\tan(\phi). \tag{3}$$

Note, however, that the inextensibility of the belt requires that the change in belt radius of the primary and secondary clutches are always in opposite directions; $\Delta r_s/\Delta r_p < 0$. A homologous vector analysis performed on the secondary clutch yields

$$z_s = 2(r_{s,eng} - r_s)\tan(\phi), \tag{4}$$

so long as the z-coordinate direction remains consistent with that used to derive (3).

2.2 Primary Clutch Mechanism

2.2.1 Force Analysis

By modeling the CVT operations as steady-state phenomena, a quasi-static analysis may be employed by neglecting all but centripetal accelerations. Figure 4 shows a schematic of the flyweight mechanism within the primary clutch.

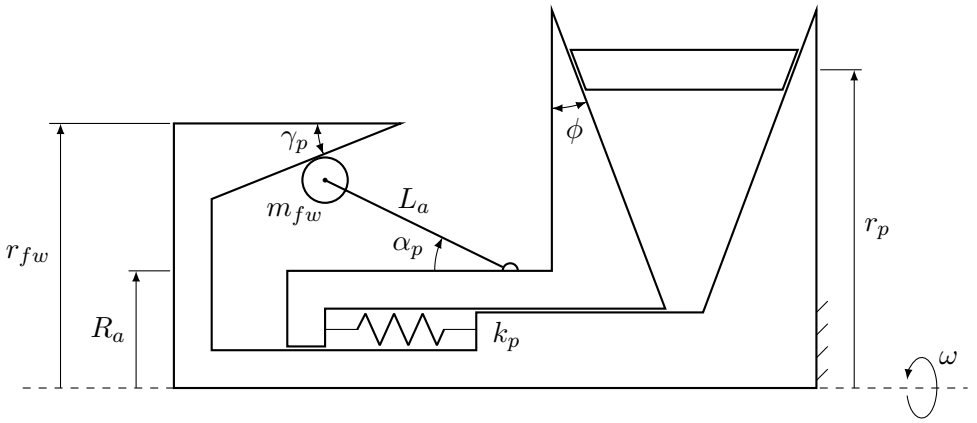

Figure 4: Primary clutch mechanism.

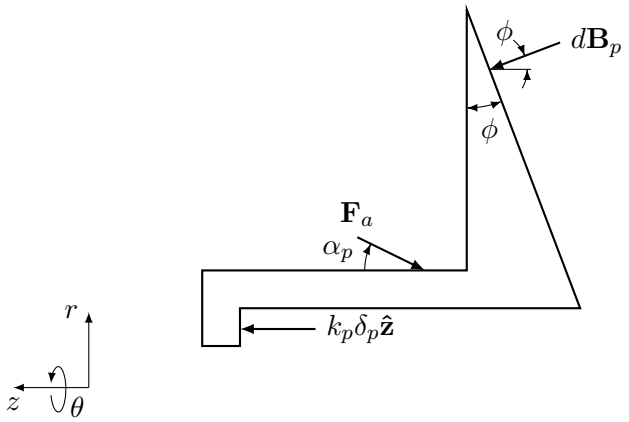

Figure 5: Forces on the moveable sheave of the primary clutch.

As shown in Figure 5, summing forces in the axial direction gives

$$-n_a F_a \cos(\alpha_p) + k_p\delta_p + \int_{\theta=\frac{\pi}{2}+\varepsilon}^{\frac{3\pi}{2}-\varepsilon} dB_p \cos(\phi) = 0,$$

where n_a is the number of flyweight arms, δ_p is the compression in the primary spring, and dB_p is the local normal force acting from the belt onto the moveable sheave at angular position θ. The total axial clamping force is then dB_p integrated over the belt wrap angle, $\theta \in [\frac{\pi}{2}+\varepsilon, \frac{3\pi}{2}-\varepsilon]$. The total spring compression can be rewritten as

$$\delta_p = \delta_{p,pre} + \delta_{p,eng} + z_p,$$

where $\delta_{p,pre}$ and $\delta_{p,eng}$ are defined as the preload compression upon assembly and the compression from the preload state to belt engagement, respectively.

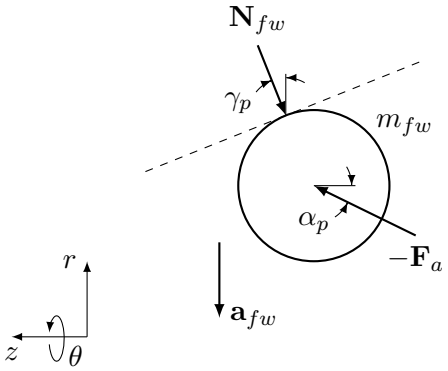

Figure 6: Forces on each flyweight of the primary clutch.

Neglecting friction, but taking into consideration the centripetal acceleration of the mass at the end of one flyweight arm, the forces shown in Figure 6 give

$$F_a(\sin(\alpha_p)\hat{\mathbf{r}} + \cos(\alpha_p)\hat{\mathbf{z}}) - N_{fw}(\cos(\gamma_p)\hat{\mathbf{r}} + \sin(\gamma_p)\hat{\mathbf{z}})) = -m_{fw}a_{fw}\hat{\mathbf{r}},$$

where N_{fw} is the normal force from the ramp onto the roller of the flyweight, F_a is the force applied by the flyweight arm, and m_{fw} is the mass of the flyweight itself. With $r_{fw} = R_a + L_a\sin(\alpha_p)$ and $a_{fw} = \omega^2 r_{fw}$, N_{fw} can be eliminated to find

$$F_a = \frac{m_{fw}\omega^2(R_a + L_a\sin(\alpha_p))}{\cos(\alpha_p)\cot(\gamma_p) - \sin(\alpha_p)}.$$

Therefore, the net axial force applied back onto the belt is

$$\int_{\theta=\frac{\pi}{2}+\varepsilon}^{\frac{3\pi}{2}-\varepsilon} dB_p\cos(\phi) = \frac{n_a m_{fw}\omega^2(R_a + L_a\sin(\alpha_p))\cos(\alpha_p)}{\cos(\alpha_p)\cot(\gamma_p) - \sin(\alpha_p)} - k_p(\delta_{p,pre} + \delta_{p,eng} + z_p). \tag{5}$$

2.2.2 Flyweight Arm Kinematics

Figure 7 displays the manner in which the flyweight rolls along the ramp as the gap between the primary sheaves decreases from the preload position.

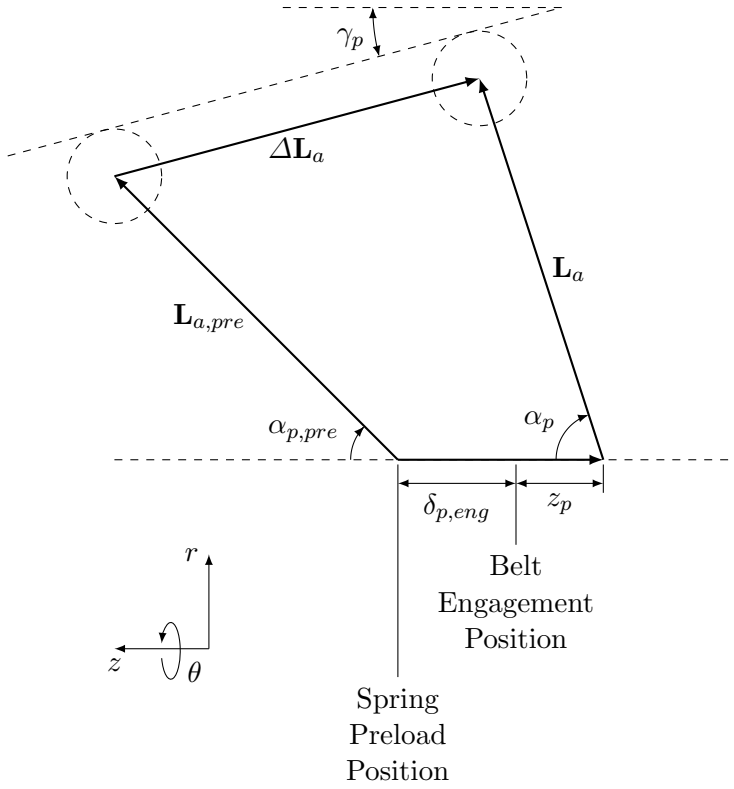

Figure 7: Motion of the flyweight and arm during shifting.

Vector analysis gives

$$-(\delta_{p,eng} + z_p)\hat{\mathbf{z}} + \mathbf{L}_a = \mathbf{L}_{a,pre} + \Delta\mathbf{L}_a,$$

which can be rewritten as

$$\begin{aligned} -(\delta_{p,eng} + z_p)\hat{\mathbf{z}} + L_a(\sin(\alpha_p)\hat{\mathbf{r}} + \cos(\alpha_p)\hat{\mathbf{z}}) \\ = L_a(\sin(\alpha_{p,pre})\hat{\mathbf{r}} + \cos(\alpha_{p,pre})\hat{\mathbf{z}}) + \|\Delta\mathbf{L}_a\|_2(\sin(\gamma_p)\hat{\mathbf{r}} - \cos(\gamma_p)\hat{\mathbf{z}}). \end{aligned}$$

Solving for $\|\Delta\mathbf{L}_a\|_2$ from the radial components gives

$$\|\Delta\mathbf{L}_a\|_2 = \frac{L_a(\sin(\alpha_p) - \sin(\alpha_{p,pre}))}{\sin(\gamma_p)}.$$

Eliminating $\|\Delta\mathbf{L}_a\|_2$ from the axial projection then yields the following relation between primary sheave displacement and flyweight arm angle:

$$z_p = L_a(\cos(\alpha_p) - \cos(\alpha_{p,pre}) + (\sin(\alpha_p) - \sin(\alpha_{p,pre}))\cot(\gamma_p)) - \delta_{p,eng}. \tag{6}$$

2.3 Secondary Clutch Mechanism

2.3.1 Force and Torque Analysis

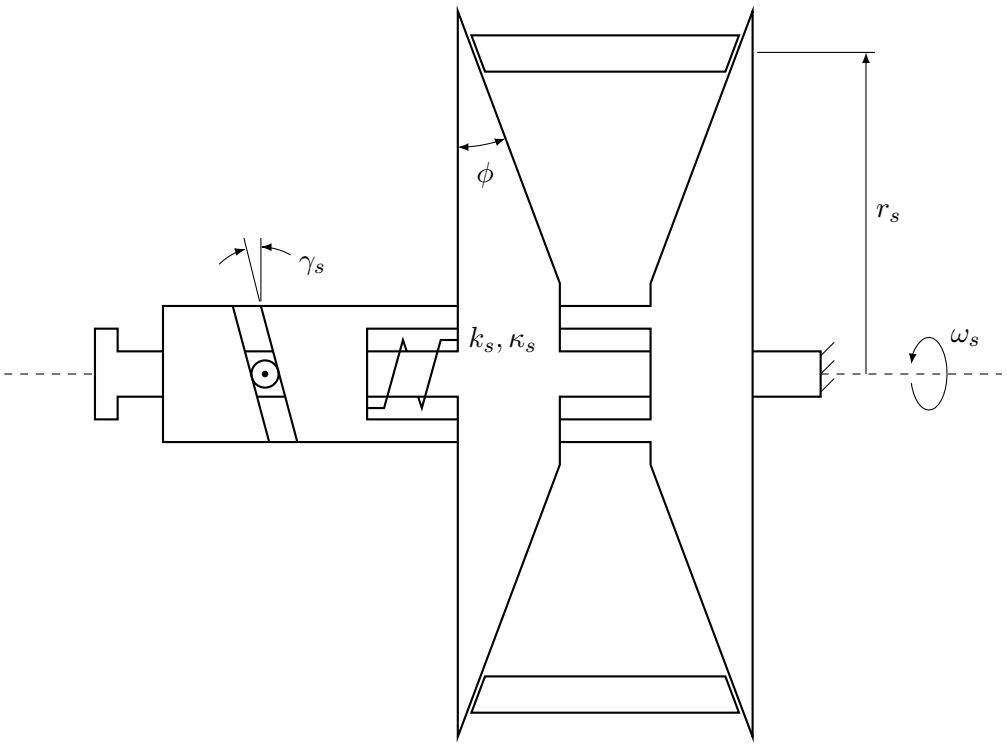

Figure 8: Secondary clutch mechanism.

Figure 8 shows a schematic of the secondary clutch mechanism. As displayed in Figure 9, summing forces on the moveable sheave in the axial direction gives

$$n_c N_c \cos(\gamma_s) + k_s \delta_s - \int_{\theta=-(\frac{\pi}{2}+\varepsilon)}^{\frac{\pi}{2}+\varepsilon} dB_s \cos(\phi) = 0,$$

where n_c is the number of cam rollers riding in the helix, δ_s is the compression in the secondary spring, and dB_s is the local normal force acting from the belt onto the moveable sheave at angular position θ. The total axial clamping force is then dB_s integrated over the belt wrap angle, $\theta \in [-(\frac{\pi}{2}+\varepsilon), \frac{\pi}{2}+\varepsilon]$. The total spring compression is

$$\delta_s = \delta_{s,pre} + z_s,$$

where $\delta_{s,pre}$ is the initial compression of the secondary spring upon assembly.

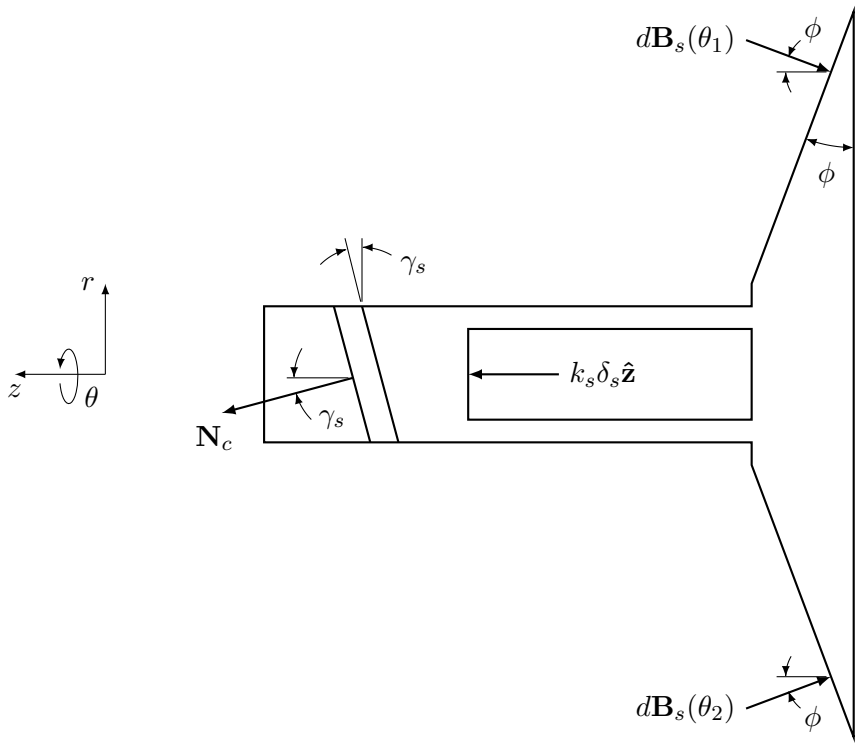

Figure 9: Forces on the moveable sheave of the secondary clutch.

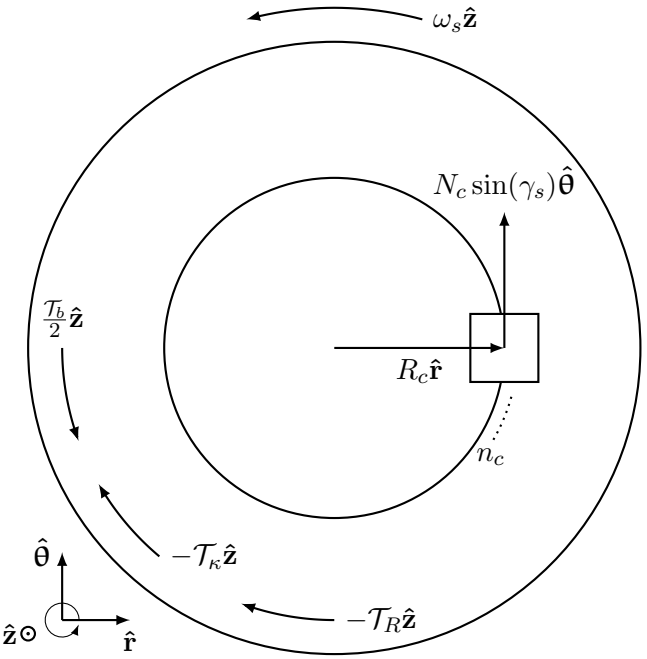

Figure 10: Torques on the axially fixed sheave of the secondary clutch.

As shown in Figure 10, the balance of torques acting on the axially fixed sheave of the secondary

clutch, about its axis of rotation, gives

$$n_c R_c N_c \sin\gamma_s + \frac{\mathcal{T}_b}{2} - \mathcal{T}_\kappa - \mathcal{T}_R = 0,$$

where $\mathcal{T}_b$ is the input torque applied by the belt, $\mathcal{T}_\kappa$ is the restoring torque due to torsion in the spring, and $\mathcal{T}_R$ is the resistive torque applied to the secondary output shaft which arises due to friction throughout the back-half of the drivetrain and gravity acting on the vehicle when traveling up inclines. Note that input torque is assumed to be split evenly between the two sheaves of the clutch. By examining the two sheaves together, the internal reactions N_c and $\mathcal{T}_\kappa$ disappear and the two external torques $\mathcal{T}_b$ and $\mathcal{T}_R$ must balance each other at steady state. Thus,

$$\mathcal{T}_b = \mathcal{T}_R.$$

Furthermore, the spring torque can be rewritten as

$$\mathcal{T}_\kappa = \kappa_s(\alpha_{s,pre} + \alpha_s),$$

where $\alpha_{s,pre}$ is the initial angular displacement of the spring, set by adjusting its torsional preload. Furthermore, α_s is the additional angle through which the moveable sheave rotates relative to the radially fixed sheave and κ_s is the torsional spring rate. Therefore, the net axial force applied back onto the belt from the moveable sheave of the secondary clutch is

$$\int_{\theta=-(\frac{\pi}{2}+\varepsilon)}^{\frac{\pi}{2}+\varepsilon} dB_s \cos(\phi) = \frac{\cot(\gamma_s)}{R_c}\Big(\frac{\mathcal{T}_R}{2} + \kappa_s(\alpha_{s,pre} + \alpha_s)\Big) + k_s(\delta_{s,pre} + z_s). \tag{7}$$

2.3.2 Helix Kinematics

As shown in Figure 11, the cam roller rides along the helix at an angle of γ_s as the sheaves rotate relative to one another. The helical constraint in turn forces the sheaves to move axially with respect to each other. This geometric constraint can be written mathematically as

$$\tan(\gamma_s) = \frac{\Delta z}{\Delta r}.$$

Note that for small rotations, $\Delta r \approx \Delta\widehat{S}$, where $\Delta\widehat{S}$ is the circular arc generated by projecting the helical path of the cam onto the $r\theta$-plane. This arc length can be expressed as

$$\Delta\widehat{S} = R_c\Delta\alpha_s.$$

Thus,

$$\tan(\gamma_s) \approx \frac{\Delta z}{R_c\Delta\alpha_s}.$$

Note that since

$$\lim_{\Delta\alpha_s\to 0} \Delta r = dr = d\widehat{S},$$

the above approximation holds exactly, and thus

$$\tan(\gamma_s) = \frac{dz}{R_c d\alpha_s}.$$

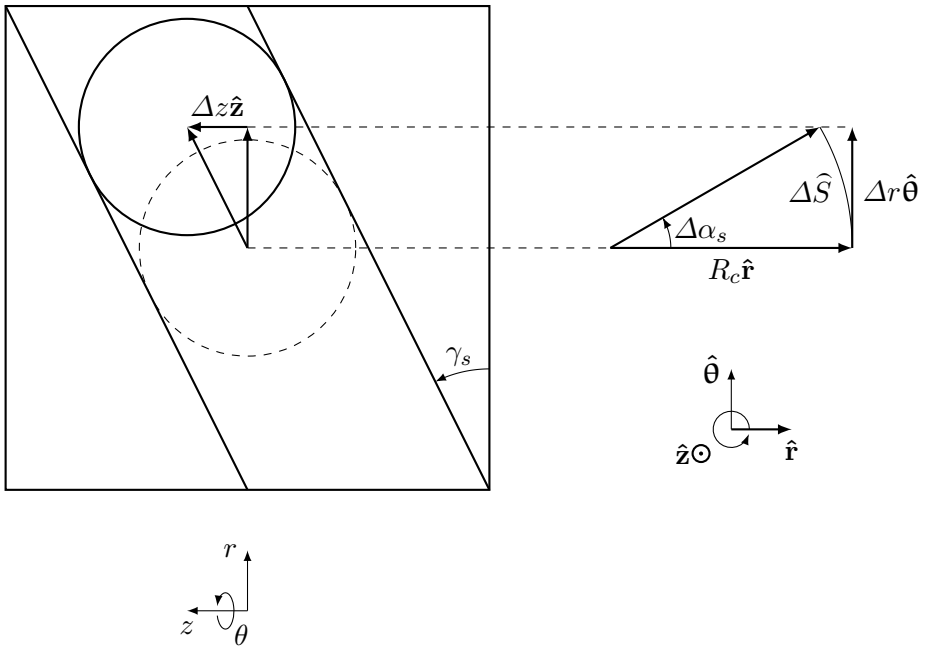

Figure 11: Helical constraint of the secondary cam rollers.

Therefore, integration over the rotation from belt engagement gives

$$\int_0^{z_s} dz = \int_0^{\alpha_s} R_c \tan(\gamma_s) d\alpha_s.$$

For constant helical angle γ_s,

$$z_s = R_c \alpha_s \tan(\gamma_s). \tag{8}$$

2.4 Uncoupled Model

Thus far, the equations governing the operation of the v-belt CVT of interest have been derived in the context of their respective subsystems. The model is defined by (1) through (8) below. Note, however, that the clamping forces of the primary and secondary clutches have yet to be coupled together. The axial compressive force applied by the primary clutch onto the belt fights against the axial compressive force applied by the secondary system, and vice versa. This coupling relationship between the two clamping forces will be developed in the following section by assuming a uniform clamping pressure, then applied to the overall model as a means of generating a MATLAB tuning program.

$$\varepsilon = \arcsin\left(\frac{r_s - r_p}{C}\right) \tag{1}$$

$$L_b = \pi(r_p + r_s) + 2(r_s - r_p)\arcsin\left(\frac{r_s - r_p}{C}\right) + 2\Big(C^2 - (r_s - r_p)^2\Big)^{1/2} \tag{2}$$

$$z_p = 2(r_p - r_{p,eng})\tan(\phi) \tag{3}$$

$$z_s = 2(r_{s,eng} - r_s)\tan(\phi) \tag{4}$$

$$\int_{\theta=\frac{\pi}{2}+\varepsilon}^{\frac{3\pi}{2}-\varepsilon} dB_p \cos(\phi) = \frac{n_a m_{fw}\omega^2(R_a + L_a\sin(\alpha_p))\cos(\alpha_p)}{\cos(\alpha_p)\cot(\gamma_p) - \sin(\alpha_p)} - k_p(\delta_{p,pre} + \delta_{p,eng} + z_p) \tag{5}$$

$$z_p = L_a(\cos(\alpha_p) - \cos(\alpha_{p,pre}) + (\sin(\alpha_p) - \sin(\alpha_{p,pre}))\cot(\gamma_p)) - \delta_{p,eng} \tag{6}$$

$$\int_{\theta=-(\frac{\pi}{2}+\varepsilon)}^{\frac{\pi}{2}+\varepsilon} dB_s \cos(\phi) = \frac{\cot(\gamma_s)}{R_c}\Big(\frac{\mathcal{T}_R}{2} + \kappa_s(\alpha_{s,pre} + \alpha_s)\Big) + k_s(\delta_{s,pre} + z_s) \tag{7}$$

$$z_s = R_c \alpha_s \tan(\gamma_s) \tag{8}$$

2.5 Coupling via Uniform Clamping Pressure

The current approach to coupling the uncoupled model will be carried out under the assumption that the pressures applied onto the belt by the clutch sheaves are independent of angular position. In other words, any element of the belt along the wrap angle of a given pulley will be subjected to a constant, uniformly distributed pressure. An arbitrary belt element and the forces applied to it are shown in Figures 12 and 13.

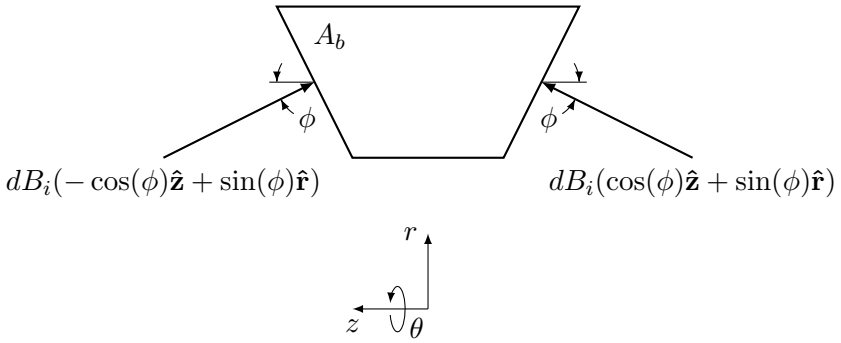

Figure 12: Forces on a belt element projected onto the rz-plane.

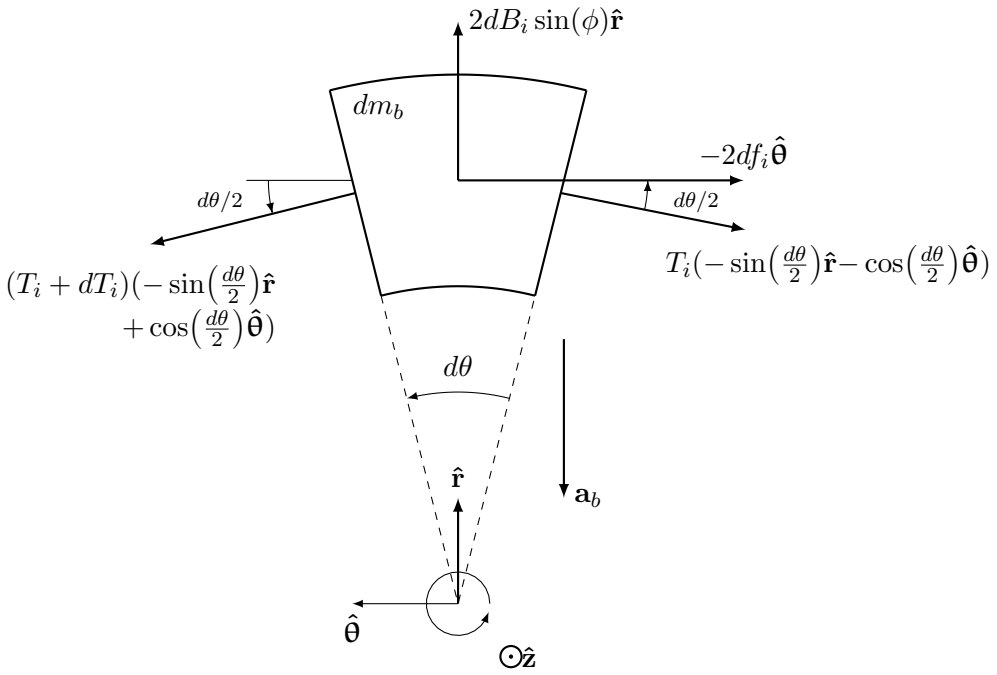

Figure 13: Forces on a belt element projected onto the $r\theta$-plane.

Note that the element of interest is in contact with the sheaves of pulley i, where $i \in \{p, s\}$ can be used to distinguish between the primary and secondary clutches, respectively. Neglecting angular and axial accelerations, force analysis gives

$$(T_i + dT_i)\Big(-\sin\Big(\frac{d\theta}{2}\Big)\hat{\mathbf{r}} + \cos\Big(\frac{d\theta}{2}\Big)\hat{\boldsymbol{\theta}}\Big) + 2dB_i \sin(\phi)\hat{\mathbf{r}} - 2df_i\hat{\boldsymbol{\theta}} \\ - T_i\Big(\sin\Big(\frac{d\theta}{2}\Big)\hat{\mathbf{r}} + \cos\Big(\frac{d\theta}{2}\Big)\hat{\boldsymbol{\theta}}\Big) = -dm_b a_b \hat{\mathbf{r}},$$

where T_i is the tension in the belt along its contact patch with pulley i, df_i is the friction force applied onto the belt from each of the sheaves, and a_b is the centripetal acceleration of the belt element. Note that through Taylor expansion, is can be shown

$$\cos\Big(\frac{d\theta}{2}\Big) \approx 1,$$

and

$$\sin\Big(\frac{d\theta}{2}\Big) \approx \frac{d\theta}{2}.$$

Therefore,

$$\Big(-T_i d\theta - dT_i\frac{d\theta}{2} + 2dB_i \sin(\phi)\Big)\hat{\mathbf{r}} + (dT_i - 2df_i)\hat{\boldsymbol{\theta}} = -dm_b a_b \hat{\mathbf{r}}.$$

Using $\overline{r}_i$ to denote the radius to the centroid of the element,

$$dm_b = \rho_b A_b \overline{r}_i d\theta,$$

where ρ_b is the mass density of the belt and A_b is its cross-sectional area. Furthermore,

$$dB_i = P_i dA_i,$$

where P_i is the normal pressure acting from the sheaves onto the belt element and dA_i is the surface area of the element of differential arc length in contact with each of the sheaves. Also note that the second-order term may be neglected; $dT_i d\theta \approx 0$. Therefore, the equations of motion become

$$(-T_i d\theta + 2P_i dA_i \sin(\phi))\hat{\mathbf{r}} + (dT_i - 2df_i)\hat{\boldsymbol{\theta}} = -\rho_b A_b \overline{r}_i d\theta a_b \hat{\mathbf{r}}.$$

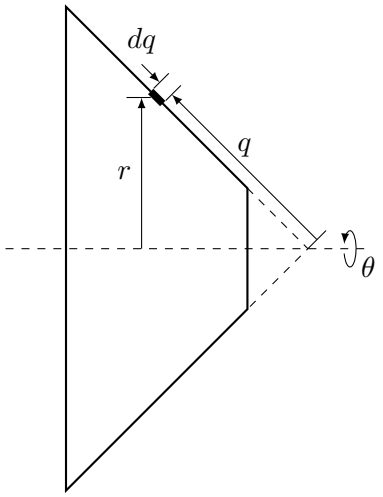

Figure 14: Conical coordinate system.

As shown in Figure 14, the contact area can be found in terms of conical coordinates. Using q to measure length along the conical sheave surface through a constant angular position, the differential surface area of a cone is given by $dA = rd\theta dq$. Thus, the area of the belt element is

$$dA_i = \int_{q=q_{i,1}}^{q_{i,2}} rd\theta dq = d\theta \int_{q=q_{i,1}}^{q_{i,2}} rdq.$$

Therefore,

$$\left(-T_i d\theta + 2P_i d\theta \int_{q=q_{i,1}}^{q_{i,2}} rdq \sin(\phi)\right)\hat{\mathbf{r}} + (dT_i - 2df_i)\hat{\boldsymbol{\theta}} = -\rho_b A_b \overline{r}_i d\theta a_b \hat{\mathbf{r}},$$

where the centripetal acceleration of the belt element is

$$a_b = \omega_i^2 \overline{r}_i.$$

Substituting this result and rearranging the radial components gives

$$T_i = \rho_b A_b (\omega_i \overline{r}_i)^2 + 2P_i \sin(\phi) \int_{q=q_{i,1}}^{q_{i,2}} rdq.$$

Note that this result is independent of angular location, and thus the tension remains constant throughout the wrap angle on the pulley. Therefore, as seen in Figure 15, the tension between the two belts must equal each other, which remains constant throughout each of the wrap angles. That is,

$$T_p = T_s,$$
$$\rho_b A_b (\omega_p \overline{r}_p)^2 + 2P_p \sin(\phi) \int_{q=q_{p,1}}^{q_{p,2}} rdq = \rho_b A_b (\omega_s \overline{r}_s)^2 + 2P_s \sin(\phi) \int_{q=q_{s,1}}^{q_{s,2}} rdq.$$

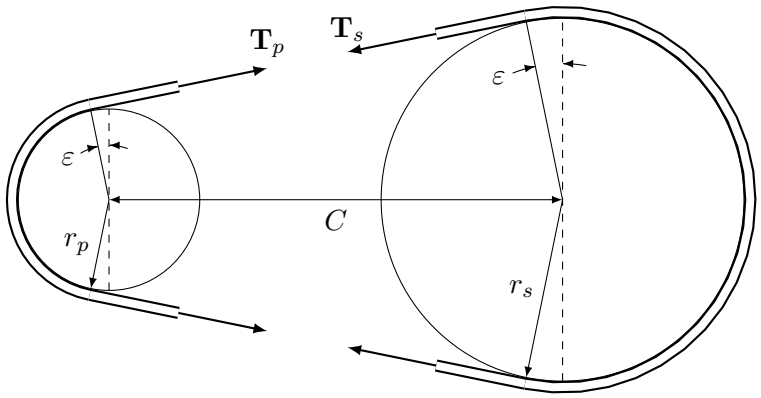

Figure 15: Primary-to-secondary belt tension relation.

Since the belt is modeled as inextensible and incompressible, each point along its length must travel with the same linear velocity. Specifically, along the line passing through the centroid of each cross-section,

$$\overline{v}_b = \omega_p \overline{r}_p = \omega_s \overline{r}_s,$$

and therefore

$$\omega_s = \frac{\overline{r}_p}{\overline{r}_s} \omega_p.$$

Substituting this result into the belt tension equality gives

$$\rho_b A_b(\omega_p \overline{r}_p)^2 + 2P_p \sin(\phi) \int_{q=q_{p,1}}^{q_{p,2}} r dq = \rho_b A_b \Big(\frac{\overline{r}_p}{\overline{r}_s}\omega_p \overline{r}_s\Big)^2 + 2P_s \sin(\phi) \int_{q=q_{s,1}}^{q_{s,2}} r dq,$$

where the centripetal terms end up canceling, leaving only the following ratio between the two pressures:

$$P_p \int_{q=q_{p,1}}^{q_{p,2}} r dq = P_s \int_{q=q_{s,1}}^{q_{s,2}} r dq.$$

The differential normal forces $dB_i = P_i dA$ can then be related by

$$\begin{aligned} dB_s &= P_s d\theta \int_{q=q_{s,1}}^{q_{s,2}} r dq \\ &= \left(P_p \frac{\int_{q=q_{p,1}}^{q_{p,2}} r dq}{\int_{q=q_{s,1}}^{q_{s,2}} r dq} \right) d\theta \int_{q=q_{s,1}}^{q_{s,2}} r dq, \\ dB_s &= P_p d\theta \int_{q=q_{p,1}}^{q_{p,2}} r dq = dB_p. \end{aligned}$$

Thus, the uniform pressure approach to coupling the two clutches results in equivalent constant-valued differential normal forces applied from both pulleys onto the belt. Substituting this result into (7),

$$\begin{aligned} \int_{\theta=-(\frac{\pi}{2}+\varepsilon)}^{\frac{\pi}{2}+\varepsilon} P_p d\theta \int_{q=q_{p,1}}^{q_{p,2}} r dq \cos(\phi) &= \frac{\cot(\gamma_s)}{R_c}\Big(\frac{\mathcal{T}_R}{2} + \kappa_s(\alpha_{s,pre} + \alpha_s)\Big) + k_s(\delta_{s,pre} + z_s), \\ P_p \int_{q=q_{p,1}}^{q_{p,2}} r dq \cos(\phi) &= \frac{\frac{\cot(\gamma_s)}{R_c}\Big(\frac{\mathcal{T}_R}{2} + \kappa_s(\alpha_{s,pre} + \alpha_s)\Big) + k_s(\delta_{s,pre} + z_s)}{\int_{\theta=-(\frac{\pi}{2}+\varepsilon)}^{\frac{\pi}{2}+\varepsilon} d\theta}. \end{aligned}$$

Substituting the same result for dB_p in (5) gives

$$\begin{aligned} \int_{\theta=\frac{\pi}{2}+\varepsilon}^{\frac{3\pi}{2}-\varepsilon} P_p d\theta \int_{q=q_{p,1}}^{q_{p,2}} r dq \cos(\phi) &= \frac{n_a m_{fw} \omega^2 (R_a + L_a \sin(\alpha_p)) \cos(\alpha_p)}{\cos(\alpha_p)\cot(\gamma_p) - \sin(\alpha_p)} - k_p(\delta_{p,pre} + \delta_{p,eng} + z_p), \\ P_p \int_{q=q_{p,1}}^{q_{p,2}} r dq \cos(\phi) &= \frac{\frac{n_a m_{fw} \omega^2 (R_a + L_a \sin(\alpha_p)) \cos(\alpha_p)}{\cos(\alpha_p)\cot(\gamma_p) - \sin(\alpha_p)} - k_p(\delta_{p,pre} + \delta_{p,eng} + z_p)}{\int_{\theta=\frac{\pi}{2}+\varepsilon}^{\frac{3\pi}{2}-\varepsilon} d\theta}. \end{aligned}$$

Note that, as with their corresponding differential normal forces, the clamping forces per unit angle are equivalent between primary and secondary clutches. Equating the two gives

$$\begin{aligned} &\frac{\frac{\cot(\gamma_s)}{R_c}\Big(\frac{\mathcal{T}_R}{2} + \kappa_s(\alpha_{s,pre} + \alpha_s)\Big) + k_s(\delta_{s,pre} + z_s)}{\int_{\theta=-(\frac{\pi}{2}+\varepsilon)}^{\frac{\pi}{2}+\varepsilon} d\theta} \\ &\qquad = \frac{\frac{n_a m_{fw} \omega^2 (R_a + L_a \sin(\alpha_p)) \cos(\alpha_p)}{\cos(\alpha_p)\cot(\gamma_p) - \sin(\alpha_p)} - k_p(\delta_{p,pre} + \delta_{p,eng} + z_p)}{\int_{\theta=\frac{\pi}{2}+\varepsilon}^{\frac{3\pi}{2}-\varepsilon} d\theta}. \end{aligned}$$

Integrating over the belt wrap angles, substituting (1), and rearranging yields the following solution function η. The goal in tuning the CVT is to manipulate the balance of forces such that $\eta \approx 0$

for the entire shift range of the CVT when subject to resistive loading $\mathcal{T}_R$. Alongside the formulas derived for the uncoupled model, this function is implemented in the MATLAB program found in Listing 1.

$$\eta \coloneqq \Big(\tfrac{\cot(\gamma_s)}{R_c}\big(\tfrac{\mathcal{T}_R}{2} + \kappa_s(\alpha_{s,pre} + \alpha_s)\big) + k_s(\delta_{s,pre} + z_s)\Big)\big(\pi - 2\arcsin\big(\tfrac{r_s - r_p}{C}\big)\big) - \Big(\tfrac{n_a m_{fw}\omega^2(R_a + L_a\sin(\alpha_p))\cos(\alpha_p)}{\cos(\alpha_p)\cot(\gamma_p) - \sin(\alpha_p)} - k_p(\delta_{p,pre} + \delta_{p,eng} + z_p)\Big)\big(\pi + 2\arcsin\big(\tfrac{r_s - r_p}{C}\big)\big) = 0. \quad (9)$$

3 Future Work

The most immediate goals for advancing this project include experimentally validating the proposed solution approach, as well as generating more coupling methods and tuning approaches. Experiments should be designed to measure the resistive torque felt at the secondary, preferably as a function of vehicle speed and incline angle. Furthermore, experiments to measure the engine speed and power output for a given set of weights should be performed in order to verify the correct operating speed for the masses output by the program. One long-term goal of interest is developing a transient response model. Models incorporating energy losses due to friction would also be of usefulness. Additionally, more realistic, nonlinear profiles for the ramp and helix angles should be experimentally measured for increased accuracy of the tuning program.

References

[1] G. Carbone, L. Mangialardi, B. Bonsen, C. Tursi, and P. A. Veenhuizen, "CVT Dynamics: Theory and Experiments," *Mechanism and Machine Theory*, vol. 42, pp. 409 – 428, 2007.

[2] G. Julió and J. S. Plante, "An Experimentally-Validated Model of Rubber-Belt CVT Mechanics," *Mechanism and Machine Theory*, vol. 46, pp. 1037 – 1053, 2015.

[3] V. A. Lubarda, "Determination of the Belt Force Before the Gross Slip," *Mechanism and Machine Theory*, vol. 83, pp. 31 – 37, 2015.

[4] R. Willis, "A Kinematic Analysis and Design of a Continuously Variable Transmission," M.S. thesis, Virginia Polytechnic Institute and State University, Blacksburg, VA, 2006.

Listing 1: MATLAB program for CVT tuning.

```
clc; clear; close all;

% Created by Brendon Anderson on 1/7/2017. Updated 2/4/2017.

%%%%%%%%%% NOTES %%%%%%%%%%
% all values are in SI units
% conversion factors and known/computed values are uppercase
% parametric variables are lowercase
% parametric functions are lowercase with appended underscore
% additional functions for repeated parameters are appended with
    additional underscore

%%%%%%%%%% CONVERSION FACTORS %%%%%%%%%%
DEG2RAD = pi/180;                % degrees to radians
FT2M = 0.3048;                   % feet to meters
IN2M = 0.0254;                   % inches to meters
LBF2N = 4.44822;                 % pounds (force) to newtons
LBM2KG = 0.453592;               % pounds (mass) to kilograms
MIN2S = 60;                      % minutes to seconds
REV2RAD = 2*pi;                  % revolutions to radians

%%%%%%%%%% KNOWN VALUES %%%%%%%%%%
ALPHA_P_PRE = 2.38*DEG2RAD;      % flyweight arm angle at preload
ALPHA_P_F = 19.05*DEG2RAD;       % flyweight arm angle at shift-out
ALPHA_S_PRE = 25*DEG2RAD;        % secondary spring torsion preload angle
C = 10.075*IN2M;                 % center to center pulley distance
DELTA_P_PRE = 0.945*IN2M;        % primary spring compression at preload
DELTA_P_ENG = 0.075*IN2M;        % primary spring compression from preload
    to belt engagement
DELTA_S_PRE = 1.34*IN2M;         % secondary spring compression at preload
GAMMA_P = 22.55*DEG2RAD;         % flyweight ramp angle
GAMMA_S = 30.5*DEG2RAD;          % helix angle
K_P = 48.14*LBF2N/IN2M;          % primary spring rate
K_S = 22.475*LBF2N/IN2M;         % secondary spring rate (compressive)
KAPPA_S = 1.8588*DEG2RAD*(1/IN2M)*(LBF2N);      % secondary spring rate (
    torsional)
L_A = 1.253*IN2M;                % flyweight arm length
N = 100;                         % grid size
N_A = 4;                         % number of flyweight arms
N_ITER = 1000;                   % number of numerical iterations
OMEGA = 3400*REV2RAD/MIN2S;      % engine rotational speed
PHI = 12.85*DEG2RAD;             % sheave angle
R_A = 1.6125*IN2M;               % radius to flyweight arm pivot
R_C = 1.6025*IN2M;               % radius to center of helical surface
R_P_ENG = 1.135*IN2M;            % primary belt radius at preload
R_P_F = 2.65*IN2M;               % primary belt radius at shift-out
R_S_ENG = 3.79*IN2M;             % secondary belt radius at preload
R_S_F = 2.0635*IN2M;             % secondary belt radius at shift-out
TAU_R = 17*LBF2N*FT2M;           % secondary resistive torque load
TOL = 10^(-6);                   % numerical tolerance

%%%%%%%%%% PARAMETRIC FUNCTIONS %%%%%%%%%%
%%% sheave displacement %%%
```

```
z_p_ = @(r_p) 2*(r_p - R_P_ENG)*tan(PHI);   % primary spring compression after belt engagement as function of primary belt radius
z_s_ = @(r_s) 2*(R_S_ENG - r_s)*tan(PHI);       % secondary sheave displacement as function of secondary belt radius

%%% flyweight arm angle (curvefit) %%%
z_p__ = @(alpha_p) L_A*((cos(alpha_p) - cos(ALPHA_P_PRE))...
    + (sin(alpha_p) - sin(ALPHA_P_PRE))*cot(GAMMA_P))...
    - DELTA_P_ENG;  % primary spring compression after belt engagement as function of flyweight arm angle
ALPHA_P = linspace(ALPHA_P_PRE,ALPHA_P_F,N)';
Z_P = z_p__(ALPHA_P);
coeff = polyfit(Z_P, ALPHA_P, 2);
alpha_p_ = @(z_p) coeff(1)*z_p.^2 + coeff(2)*z_p + coeff(3);    % flyweight arm angle as function of primary spring compression after belt engagement

%%% belt radius kinematics (curvefit) %%%
l_b_ = @(r_p, r_s) pi*(r_p + r_s) + 2*(r_s - r_p).*asin((r_s - r_p)/C)...
    + 2*sqrt(C^2 - (r_s - r_p).^2);     % belt length as function of pulley radii
L_B = l_b_(R_P_ENG, R_S_ENG);           % overall belt length
R_P = linspace(R_P_ENG,R_P_F,N)';
R_S = ((R_S_ENG + R_S_F)/2)*ones(length(R_P),1);    % initial guesses for secondary radii
E = 1;                                  % initialize error
ii = 0;                                 % initialize counter
f_ = @(r_p,r_s) l_b_(r_p,r_s) - L_B;    % function for newton-raphson method
df_ = @(r_p,r_s) pi + 2*asin((r_s - r_p)/C)...
    + 2*(r_s - r_p)./(C*sqrt(1 - ((r_s - r_p)/C).^2))...
    - 2*(r_s - r_p).*(C^2 - (r_s - r_p).^2);    % df/dr_s for jacobian
while (max(abs(E)) > TOL) && (ii < N_ITER)      % iteration for newton-raphson method
    ii = ii + 1;
    E = -diag(df_(R_P,R_S))\f_(R_P,R_S);
    R_S = R_S + E;
end
coeff = polyfit(R_P, R_S, 2);
r_s_ = @(r_p) coeff(1)*r_p.^2 + coeff(2)*r_p + coeff(3);    % secondary radius as function of primary radius

%%% axial compressive force %%%
f_p_z_ = @(alpha_p, m_fw, z_p) (N_A*m_fw*(OMEGA^2)*(R_A + L_A*sin(alpha_p))...
    *cos(alpha_p))/(cos(alpha_p)*cot(GAMMA_P) - sin(alpha_p))...
    - K_P*(DELTA_P_PRE + DELTA_P_ENG + z_p);    % primary compressive force as function of flyweight arm angle, flyweight mass, and primary spring compression
f_s_z_ = @(tau_j, z_s) K_S*(DELTA_S_PRE + z_s)...
    + (tau_j + 2*KAPPA_S*(ALPHA_S_PRE + z_s/(R_C*tan(GAMMA_S))))...
    /(2*R_C*tan(GAMMA_S));                  % secondary compressive force as function of secondary inertial torque and secondary sheave displacement
```

```
90
91  %%%%%%%%%% SOLUTION APPROACH: UNIFORM PRESSURE DISTRIBUTION %%%%%%%%%%
92  %%% primary to secondary coupling %%%
93  eta_ = @(f_p_z, f_s_z, r_p, r_s) (pi + 2*asin((r_s - r_p)/C))*f_p_z...
94      - (pi - 2*asin((r_s - r_p)/C))*f_s_z;       % coupling equation
95
96  %%% flyweight mass for average inertial torque at average belt position
        %%%
97  R_P_AVG = mean([R_P_ENG, R_P_F]);       % average belt position (middle of
        shift)
98  M_FW = 0.1;                             % initial guess for flyweight mass
99  E = 1;                                  % initialize error
100 ii = 0;                                 % initialize counter
101 f_ = @(f_p_z, f_s_z, r_p, r_s) eta_(f_p_z, f_s_z, r_p, r_s);    % function
        for newton-raphson method
102 df_ = @(alpha_p, r_p, r_s, z_p) (pi + 2*asin((r_s - r_p)/C))...
103     *f_p_z_(alpha_p, 1, z_p);       % df/dr_s for jacobian
104 Jinv = -1./df_(alpha_p_(z_p_(R_P_AVG)),...
105     R_P_AVG, r_s_(R_P_AVG), z_p_(R_P_AVG));     % inverse of jacobian
106 while (max(abs(E)) > TOL) && (ii < N_ITER)      % iteration for newton-
        raphson method
107     ii = ii + 1;
108     E = Jinv*f_(f_p_z_(alpha_p_(z_p_(R_P_AVG)), M_FW, z_p_(R_P_AVG)),
            f_s_z_(TAU_R, z_s_(r_s_(R_P_AVG))), R_P_AVG, r_s_(R_P_AVG));
109     M_FW = M_FW + E;
110 end
111 disp(['M_FW = ', num2str(M_FW), ' kg']);
```